Environmental Science Nano

ROYAL SOCIETY OF CHEMISTRY

PAPER

View Article Online
View Journal

Cite this: DOI: 10.1039/d1en00433f

Natural organic matter adsorption conditions influence photocatalytic reaction pathways of phosphate-treated titanium dioxide nanoparticles†

Riya A. Mathew,[a] Gang Wu,[b] Ye Zhang,[cd] Sheyda Shakiba,[a] Yan Yao,[cd] Ah-Lim Tsai[b] and Stacey M. Louie *[a]

Received 11th May 2021,
Accepted 3rd July 2021

DOI: 10.1039/d1en00433f

rsc.li/es-nano

Titanium dioxide (TiO_2) nanoparticles have been widely studied for water treatment applications; however, natural organic matter (NOM) is often reported to hamper the efficiency of the nanoparticles toward the degradation of target pollutants. Phosphate treatment has been proposed as a potentially facile solution to this problem, as phosphate competes for TiO_2 surface sites to diminish the NOM adsorption. However, the potential importance of the conditions of the NOM exposure and the residual NOM remaining after phosphate treatment have not been fully explored. Here, we investigate the reactivity of phosphate-treated TiO_2 nanoparticles with NOM coatings adsorbed from two background water chemistries, deionized water (TiO_2–NOM_{DIW}) and moderately hard water (TiO_2–NOM_{MHW}). Thorough characterization by size exclusion chromatography revealed that the adsorbed NOM was only partially displaced after phosphate treatment, with a higher adsorbed mass and wider variety of NOM species persisting on TiO_2–NOM_{MHW} compared to TiO_2–NOM_{DIW}. Although the remaining adsorbed NOM did not significantly influence the degradation rate of phenol as a model pollutant, remarkably distinct effects were observed in the degradation of catechol as an oxidative byproduct of phenol, with TiO_2–NOM_{MHW} hindering catechol degradation and TiO_2–NOM_{DIW} accelerating catechol degradation. The suppressed reactivity for TiO_2–NOM_{MHW} was attributed to hindrance of the physical adsorption of catechol to the TiO_2 surface by the NOM_{MHW} layer as well as changes in the reactive oxygen species profile as measured by electron paramagnetic resonance (EPR) spectroscopy, whereas the enhanced reactivity for TiO_2–NOM_{DIW} was attributed to higher hole formation, suggesting participation of the NOM_{DIW} layer in electron transfer processes. This research highlights the critical importance of the NOM surface coating in directing the mechanisms for pollutant degradation in photocatalytic nano-enabled water treatment applications.

Environmental significance

Titanium dioxide (TiO_2) nanoparticles are of interest for photocatalytic water treatment, but natural organic matter (NOM) often inhibits their reactivity. Although phosphate treatment has been proposed to mitigate NOM fouling, this study identifies that differences in NOM adsorption from different water chemistries – deionized water (DIW) and moderately hard water (MHW) – persist even after phosphate treatment. Furthermore, the different NOM layers impart divergent influences on the nanoparticle reactivity: more extensive NOM adsorption from MHW inhibits reactivity by occupying adsorptive sites and modifying the reactive oxygen species profile, whereas a thinner NOM layer adsorbed from DIW promotes reactivity through enhanced hole generation. These mechanistic findings are broadly useful to understand the critical role of surface chemistry on the photocatalytic reactivity of nanomaterials.

[a] Department of Civil and Environmental Engineering, University of Houston, Houston, TX 77004, USA. E-mail: slouie@uh.edu; Fax: +713 743 4260; Tel: +713 7438646
[b] Department of Internal Medicine, McGovern Medical School, University of Texas Health Science Center at Houston, Houston, TX 77030, USA
[c] Department of Electrical and Computer Engineering, University of Houston, Houston, TX 77004, USA
[d] Texas Center for Superconductivity at the University of Houston, Houston, TX 77204, USA

† Electronic supplementary information (ESI) available: Additional NP characterization (DLS, polydispersity index and zeta potential measurements), XRD and ATR-FTIR spectra, SEC chromatograms and method information, LC-QTOF methods and data, and probe reactivity experiments. See DOI: 10.1039/d1en00433f

Introduction

Titanium dioxide (TiO_2) nanoparticles (NPs) have widely been evaluated as photocatalysts for water treatment for their potential to degrade recalcitrant pollutants *via* the generation of reactive oxygen species (ROS) upon ultraviolet (UV) irradiation.[1] However, the reaction efficiency can be hampered in realistic use conditions, as both background electrolytes and natural organic matter (NOM) in the water can scavenge ROS, form secondary radical species, attenuate light radiation or adsorb to the NP to compete with the

contaminant of interest for active sites at the NP surface.[2–12] Alternatively, NOM can induce enhanced reactivity or photosensitization through excitation to triplet state NOM.[2,13–16] Kang *et al.* distinguished that photoreactivity was enhanced in the presence of low concentrations of NOM but suppressed in high concentrations of NOM.[6] To counter losses in efficiency, phosphate modification of TiO_2 has been proposed. The adsorption of phosphate can confer colloidal stability through electrostatic repulsion.[3] Furthermore, although prior reports vary as to whether the phosphate itself promotes[17,18] or inhibits[3] ROS generation, Long *et al.* identified a major benefit of phosphate to mitigate the inhibitory effect of humic acid (HA) through competitive adsorption or displacement of HA from the TiO_2 surface.[18] Under certain conditions (high pH, low HA concentration), a slight enhancement of phenol degradation was also observed and was credited to the changes in the conformation and binding mode of HA by phosphate, leading to increased electron transfer and reduced hole scavenging.[18]

Given the importance of the properties of the adsorbed NOM layer in promoting or diminishing the efficiency of the TiO_2 NPs in water treatment, a more thorough investigation is warranted into whether the NOM adsorption conditions impact the potential for phosphate treatment to restore the reactivity of NOM-fouled NPs. NOM adsorption onto TiO_2 is well known to depend not only on the type of NOM (*e.g.*, fulvic *versus* humic fractions) and its concentration but on the water chemistry, pH, presence of background electrolytes, and ionic strength.[19,20] In particular, the presence of Ca^{2+} can induce higher adsorption of NOM by cationic bridging to the TiO_2 surface or entanglement of the NOM.[21,22] Adsorptive fractionation of NOM on TiO_2 can also occur, with higher molecular weight species from Suwannee River NOM adsorbed in moderately hard water.[23] Higher molecular weight NOM species with higher aromaticity have been reported to have the greatest influence on the inhibition of TiO_2 NP photoreactivity.[7] However, it is currently unknown whether the initial adsorption conditions of the NOM, and the subsequent differences in the adsorbed mass and adsorptive fractionation of the NOM, will have persistent effects on the photoreactivity of the TiO_2 NPs, or whether any differences are eliminated upon subsequent phosphate treatment that could displace the adsorbed NOM.

A further research gap remains from prior studies on phosphate-treated TiO_2 NPs that only monitored degradation of the "parent" contaminant (*e.g.*, phenol), but did not evaluate the formation or degradation of reaction byproducts that may have different reaction pathways. For example, phenol oxidizes to form primarily two initial isomers: hydroquinone (HQ) and catechol. Although phenol has been reported to show primarily hydroxyl radical mediated degradation,[17,24] catechol has been reported to participate in hole mediated pathways,[17] and in general, the generation or degradation of byproducts can differ based on their selectivity to specific types of ROS.[25] Therefore, it is currently unclear whether the influences of phosphate and NOM on phenol degradation can be generalized to other compounds, including phenol byproducts.

The objective of this paper is to investigate the mechanisms by which different NOM coatings influence the photoreactivity of TiO_2 NPs by probing the photodegradation of phenol and its two immediate byproducts, catechol and hydroquinone. Bare TiO_2 NPs are compared to those coated with NOM in deionized water (DIW) and moderately hard water (MHW), with all NPs subsequently undergoing phosphate treatment. The adsorbed layers were thoroughly characterized during both the NOM adsorption and phosphate treatment processes using size exclusion chromatography (SEC) for adsorbed mass and molecular weight fraction, as well as *in situ* Fourier transform infrared (FTIR) spectroscopy for the functional moieties. The myriad potential mechanisms for differences in the photoreactivity were then evaluated, including the influence of the surface coatings on the physical adsorption of the contaminants to the NP surface, as well as the production of holes and different types of ROS, including hydroxyl radical ($OH^{\bullet}$) and singlet oxygen ($^1O_2$), as measured in further experiments using probe compounds and electron paramagnetic resonance (EPR) spectroscopy. Overall, this research provides an improved mechanistic understanding of the importance of the NOM adsorbed layer properties on the reactivity and reaction pathways expressed by phosphate-treated TiO_2 NPs.

Materials and methods

Chemical reagents

Phenol (99.5%, Acros Organic, NJ, USA), hydroquinone (99%, Alfa Aesar, Ward Hill, MA, USA) and catechol (99%, Alfa Aesar, Ward Hill, MA, USA) were used as target compounds. Titanium dioxide (TiO_2) NPs (Standard Reference Material 1898) were obtained from the National Institute of Standards and Technology (NIST) (Gaithersburg, MD, USA). The TiO_2 NPs are composed of 76% anatase with primary particle size of 19 ± 2 nm and 24% rutile with primary particle size of 37 ± 6 nm.[26] Suwannee River NOM (Cat. No. 2R101N) was procured from the International Humic Substances Society (Saint Paul, MN, USA); the bulk elemental and functional group composition are provided in the ESI,† and the molar mass distribution was measured herein. Stock solutions of NOM were prepared at 1 g L^{-1} in deionized water and adjusted to pH ≈ 7 using 1 M and 0.1 M NaOH. Calcium chloride ($CaCl_2$) (>97%, anhydrous, ACS grade, Sigma-Aldrich, St. Louis, MO, USA) and sodium bicarbonate ($NaHCO_3$) (>99.7%, ACS grade, Sigma-Aldrich, St. Louis, MO, USA) were used to prepare the moderately hard water matrix, and potassium phosphate monobasic anhydrous (KH_2PO_4) (ACS grade, Amresco, Solon, OH, USA) and sodium phosphate dibasic heptahydrate ($Na_2HPO_4{\cdot}7H_2O$) (ACS grade, Amresco, Solon, OH, USA) for the phosphate buffer. 0.1 M or 1 M HCl (ACS reagent, Sigma-Aldrich) or NaOH (Sigma-Aldrich) were used for pH adjustment.

Potassium iodide (KI) (99.9%, Alfa Aesar, Ward Hill, MA, USA) and furfuryl alcohol (FFA) (98%, Sigma Aldrich, St.

Louis, MO, USA) were used as probe compounds for holes and $^1O_2$, respectively.[3,27,28] Iodine (0.025 N) and starch indicator (1% (w/v)) (both from VWR International, Radnor, PA, USA) were used for calibration and as an indicator, respectively, to evaluate KI oxidation. For EPR measurements, 5-tert-Butoxycarbonyl-5-methyl-1-pyrroline-N-oxide (BMPO, ≥99%, Enzo Life Science, Farmingdale, NY, USA) was used as a spin trap. For LC measurements, acetic acid (glacial, Macron Fine Chemicals, Radnor, PA, USA) and LC-MS grade water and methanol (OmniSolv, MilliporeSigma, Burlington, MA, USA) were used to prepare the mobile phase.

Preparation of NP stock suspensions

TiO_2 stock suspensions (2 g L^{-1}) were freshly prepared for each individual experiment in 15 mL of DIW using an adapted dispersion protocol:[26] 3 mL of DIW was added to 30 mg TiO_2 powder, bath sonicated for 30 seconds to form a slurry (Branson CPX1800H, Danbury, CT, USA), followed by the addition of 4.5 mL DIW and probe sonicated for 15 min at an 80% pulse cycle (8 s on, 2 s off) (Fisherbrand Model 120 Sonic Dismembrator, Fisher Scientific, Hampton, NH, USA), and finally dilution with 7.5 mL to the desired concentration and volume. The multiple stages of wetting, sonication, and dilution were identified in preliminary experiments to yield reproducible dispersions, where the hydrodynamic size of the NP stocks was verified on each stock preparation using dynamic light scattering (DLS) (Zetasizer Nano ZS, Malvern Instruments, Malvern, United Kingdom) upon diluting the NPs to 0.1 g L^{-1} in 1 mM NaCl. The measured *z*-average and volume-weighted average diameters were 162 ± 7 nm and 119 ± 7 nm, respectively, for 20 independent batches.

Preparation and phosphate treatment of NOM-coated and bare TiO_2 NPs

The stock NP suspensions were used to prepare NOM-coated TiO_2 NPs (0.5 g L^{-1} NPs and 0.2 g L^{-1} NOM) in two different water matrices – deionized water (DIW) and a simplified moderately hard water (MHW) comprised of 0.85 mM $CaCl_2$ and 1.2 mM $NaHCO_3$. The measured pH was ≈7 in DIW and ≈7.5 in MHW during the adsorption (after diluting the TiO_2 stock suspension and mixing with the pH-adjusted NOM stock), *i.e.*, the pH was near the isoelectric point of 7 for the bare TiO_2.[26] All TiO_2 suspensions (bare and coated) were rotated end-over-end at 25 rpm for approximately 20 hours to equilibrate, then centrifuged at 9000 rpm (9418*g*) for 15 min (Sorvall Legend XTR, Thermo Scientific, Waltham, MA, USA), and the supernatant was removed for total organic carbon (TOC) and SEC analysis of the unadsorbed NOM. The NPs were then washed twice into 10 mM phosphate buffer (pH 8, 1.4 mM KH_2PO_4 and 8.6 mM Na_2HPO_4) by adding phosphate buffer equal to the volume of supernatant collected, followed by centrifugation and collection of supernatants from each wash for SEC analysis. The NPs were resuspended in phosphate buffer by bath sonication for 1 to 2 min. Hydrodynamic sizes of the uncoated and NOM-coated TiO_2 suspensions were measured after phosphate treatment and further dilution to 0.1 g L^{-1} and verified to be similar to that of the stock suspension (see Results and discussion). The zeta potentials were also measured by electrophoretic light scattering (method and results in the ESI†).

To prepare uncoated (bare) TiO_2 NPs, the NP preparation was designed to be as comparable to the NOM coating conditions as possible while avoiding any extensive agglomeration that could influence the reactivity. For the DIW condition, the NP stock was diluted to 0.5 g L^{-1} in DIW at the "natural" pH of the suspension (pH 5 after dilution). Note that the uncoated TiO_2 NPs could not be prepared at pH 7 as in the NOM coating procedure, because the uncoated NPs rapidly agglomerate at their isoelectric point of ≈7.[26] Similarly, an uncoated control could not be prepared in the complete MHW matrix because Ca^{2+} induces rapid formation of agglomerates. However, to investigate the potential influence of HCO_3^- adsorption from the MHW, phenol degradation studies were also conducted on bicarbonate-exposed TiO_2 NPs prepared in 1.2 mM $NaHCO_3$. In order to achieve relatively unagglomerated suspensions in this background, the 2 g L^{-1} stock was prepared by slurrying the TiO_2 powder in 0.15 mL of alkaline solution (1 mM NaOH) instead of DIW, then continuing with the same preparation reported above, such that the NPs were not taken through the isoelectric point upon being added to the $NaHCO_3$ solution (final pH ≈ 9). All uncoated NPs (DIW or bicarbonate matrix) were then taken through the same 20 h rotation, centrifugation, and phosphate washing steps, resulting in all NPs (coated and uncoated) in the same background water chemistry (10 mM phosphate, pH 8) for the photoreactivity studies. The uncoated NPs were also probe sonicated for 15 min to redisperse agglomerates after centrifuging.

Attenuated total reflectance-Fourier transform infrared (ATR-FTIR) spectroscopy

ATR-FTIR spectroscopy was used to probe the functional groups and interactions between TiO_2 and inorganic ions in the different media (DIW *vs.* MHW), NOM and the salts in DIW *vs.* MHW, and the NOM adsorbing to the TiO_2 NPs in DIW *vs.* MHW before and after displacement by phosphate. All measurements were collected on a Nicolet iS50 FTIR spectrometer, (ThermoFisher Scientific, Waltham, MA, USA) on a diamond/ZnSe single reflection ATR crystal (PIKE Technologies, Fitchburg, WI, USA). Spectra were collected from 4000 to 800 cm^{-1} with a resolution of 2 cm^{-1} and averaged over 200 scans. The NOM samples without TiO_2 were collected as supernatants from centrifuged samples as prepared for the photoreaction experiments and processed as described in the ESI.† For the TiO_2 samples, changes in the surface chemistry of the TiO_2 in the presence of the various water chemistry were monitored by *in situ* ATR-FTIR spectroscopy. First, 6 μL of TiO_2 stock suspension (2 g L^{-1} in DIW) was dried onto the ATR crystal. Four separate *in situ*

experiments were conducted to expose the TiO_2 to the different conditions: (1) DIW followed by (→) phosphate buffer (pH 8) to identify adsorbed phosphate; (2) DIW → MHW → phosphate buffer to identify adsorbed bicarbonate and displacement by phosphate; and (3) DIW → NOM in DIW → phosphate and (4) MHW → NOM in MHW → phosphate buffer to evaluate NOM adsorption and displacement by phosphate. For experiments 1 and 2, 40 μL of the salt solutions were pipetted over the TiO_2 NPs, spectra were collected every 10 minutes for 30 minutes total, then the overlying solution was pipetted away to replace with the following solution and spectra collected similarly. For experiments 3 and 4, after taking spectra in the background electrolyte as noted, 60 μL of NOM in the background solution was applied, and the NOM adsorption spectra were collected every 10 minutes for 60 minutes; finally, desorption was monitored after two phosphate washes with spectra collected every 10 minutes for 20 minutes in each wash. To process the data, the background spectrum for subtraction was selected from a prior step to evaluate the influence of each change in water chemistry.

Total organic carbon (TOC) and size exclusion chromatography (SEC) analysis

The adsorbed mass of NOM was evaluated by solution depletion, in which the unadsorbed concentration in the supernatants from the adsorption procedure are subtracted from the initial concentration to compute the adsorbed concentration. Supernatants from the two subsequent phosphate washes were also collected to evaluate displacement of the NOM by the phosphate. The masses of all supernatants were weighed and utilized to correct for NOM in the remaining volume of supernatant from the prior wash, on the results measured in the subsequent wash.

Both batch TOC measurements and SEC analyses were conducted. TOC was measured on a Shimadzu TOC-L analyzer with 50 μL sample injection followed by addition of sulfuric acid for inorganic carbon removal, oxidation of the organic carbon on a Pt catalyst at 680 °C, sparging with air (zero gas with <1 ppm total hydrocarbon content, <6 ppm water, <1 ppm CO_2, and 20 to 22% oxygen, Matheson Tri-Gas, Irving, TX, USA), and quantification on a non-dispersive infrared detector. SEC analyses were performed on an Agilent 1290 Infinity liquid chromatography (LC) system (Agilent Technologies, Santa Clara, CA, USA) equipped with a Superdex 75 10/300 GL SEC column (GE Healthcare, Chicago, IL, USA), Agilent 1260 Infinity UV-vis diode array detector, and OptiLab T-rEX differential refractive index (dRI) detector (Wyatt Technologies, Santa Barbara, CA, USA). The mobile phase was 4 mM phosphate buffer (pH 7) with 25 mM NaCl (ref. 23 and 29–31) at 0.5 mL min^{-1} flow rate, the sample injection volume was 100 μL, and the UV detector was set to monitor the 280 nm wavelength for aromatic compounds or compounds with >3 conjugated double bonds. The data analysis to evaluate adsorption and displacement are described in the ESI.†

Phenol photodegradation experiments

The photocatalytic degradation of phenol was evaluated at two starting concentrations (50 mg L^{-1} and 20 mg L^{-1}) by the various TiO_2 NPs (0.1 g L^{-1}) in the 10 mM phosphate buffer; NP-free controls were also irradiated for evaluation. Irradiation was carried out on 10 mL of sample in quartz vials using a UV reactor (Rayonet RMR-600, Southern New England Ultraviolet Co., Branford, CT, USA) with eight fluorescent UV lamps with wavelength centered at 350 nm and total irradiance of 5.0 ± 0.2 mW cm^{-2} measured in the UVA/UVB range (UV513AB light meter, GeneralTools, New York, NY, USA), in an annular rotator with 8 vial positions and a cooling fan. In every experiment, four dark (foil-wrapped) vials were placed alternately with four UV-irradiated vials in the reactor as "dark controls" to evaluate any thermal degradation or other losses of phenol. Samples were collected at set intervals over a total duration of 300 min. Prior to sample collection, the vial was inverted three times to homogenize. The pH of all samples was measured before and after the experiments. The collected samples were centrifuged at 13 000 rpm (11 337*g*) for 15 min to pellet the NPs (Eppendorf MiniSpin Plus, Enfield, CT, USA), and the supernatant was filtered through 0.22 μm PTFE syringe filters (4 mm diameter, MicroSolv Technology, Leland, NC, USA) to remove any remnant NPs. The samples were analyzed for phenol and the degradation byproducts by LC analysis as follows.

Quantification of phenol and degradation byproducts by liquid chromatography (LC)

All samples were quantified for phenol and its two immediate byproducts (catechol and hydroquinone) by LC analysis. These byproducts were selected for quantitative analysis based on their initial identification by LC-quadrupole time-of-flight (QTOF) mass spectrometry (ESI† Table S1) and the availability of commercial material to prepare calibration standards for quantification. The LC analysis was conducted on an Agilent 1260 Infinity II system equipped with an Agilent Zorbax Eclipse Plus RRHD C_{18} column (2.1 × 50 mm, 1.8 μm). The sample injection volume was 5 μL and flow rate was 0.3 mL min^{-1}. The mobile phase solvents were (A) 0.01% acetic acid in LC-MS grade water and (B) methanol, and compounds were separated using a gradient elution from 95% A (5% B) to 85% A (15% B) over 10 minutes. Subsequently, the composition was ramped to 5% A (95% B) over 2 min and held for 3 min to flush, then ramped back to 95% A (5% B) over 2 min and held for 6 min to re-equilibrate at the initial composition. All compounds were quantified by the UV peak area at 272 nm as the peak wavelength for phenol.

Quantification of the phenol, catechol, and hydroquinone adsorption onto the TiO_2 NPs

The adsorption of phenol, catechol, and hydroquinone to the various phosphate-treated TiO_2 NPs was measured to evaluate any differences in available adsorption sites for the different

surface chemistry. Because the adsorbed masses of the three compounds were low, the phosphate-washed TiO_2 NPs were concentrated by resuspending the 15 mL of initial suspension (0.5 g L^{-1} NPs) to only 2 mL after the last wash (3.75 g L^{-1} NPs). Then, phenol, catechol, or hydroquinone were spiked into the NPs at 5 mg L^{-1}. Samples were allowed to rotate for 3 hours, and the supernatant after centrifugation was filtered and analyzed by LC as above.

Identification and evaluation of holes and ROS production

The phosphate-treated TiO_2 NPs were evaluated for holes or $^1O_2$ generation by conducting photodegradation experiments as above with probe compounds (KI for holes, and furfuryl alcohol (FFA) for $^1O_2$) instead of phenol. The KI assay was performed using 5 mM KI with samples collected after 0, 15, 30, 45 and 60 min of UV exposure. The I_2 oxidation product was quantified using the starch-iodine assay by mixing 0.5 mL of sample with 0.75 mL of starch solution in a 2 mL centrifuge tube and removing the NPs by centrifugation. The sample was stored under ice pack and analyzed within one hour after centrifugation. 0.7 mL of supernatant was transferred to a quartz cuvette and the absorbance at 585 nm was measured using UV-2600 spectrophotometer (Shimadzu, Columbia, MD, USA). The generation of singlet oxygen was analyzed by quantifying FFA (15 mM initial concentration) over 60 min of UV irradiation using the same LC gradient as in the phenol degradation experiment and quantifying the FFA against external calibration standards using the UV signal at 230 nm.

All phosphate-washed NPs were prepared for EPR analysis by coating as above and concentrating to 3.75 g L^{-1} by resuspending the pelleted TiO_2 NPs in a lower volume of 10 mM phosphate at the end of the last wash step. Then, the TiO_2 NPs were diluted to 1 g L^{-1} in 10 mM phosphate and spiked with 5 mM BMPO for EPR measurements. The samples were placed on a stir plate and irradiated by top-down UV exposure using a Spectroline MiniMax lamp holder (Spectronics Corp., Westbury, NY, USA) equipped with the same 4 W UV lamp as in the phenol photoreaction experiments, positioned ≈2.8 cm above the sample (measured irradiance of ≈4.67 mW cm^{-2}). After 10 min exposure, samples were transferred into Kimble micro capillary pipets (50 μL, DWK Lifer Sciences, Mainz, Germany) and sealed with Critoseal (Leica Microsystems, Wetzlar, Germany) for EPR measurements. Room temperature EPR measurements were conducted using a Bruker EMX X-band EPR spectrometer (Billerica, MA, USA). Typical parameters used were: frequency, 9.32 GHz; modulation frequency, 100 kHz; modulation amplitude, 0.1–0.3 G; microwave power, 20 mW; time constant, 327.7 ms.

Results and discussion

Characterization of TiO_2 NPs with NOM coatings and after phosphate treatment

All TiO_2 stock suspensions and phosphate-treated TiO_2 NPs – either uncoated (denoted "TiO_2–no NOM") or with NOM coatings adsorbed from DIW or MHW (denoted "TiO_2–NOM_{DIW}" and "TiO_2–NOM_{MHW}", respectively) – were evaluated by DLS for their hydrodynamic size and polydispersity index (PDI) (ESI† Fig. S1a and b). All of the phosphate-treated NPs showed good redispersibility relative to the original stock suspension with mean PDI < 0.2. The pH and zeta potentials before and after phosphate washes are also provided in ESI† Fig. S1c. Acidic residues on the TiO_2 material from the manufacturing process[26] resulted in a stock dispersion pH of 5, which is lower than the isoelectric point of ≈7, and hence a positive surface charge for the bare TiO_2 NPs in DIW (before phosphate treatment). On the other hand, the TiO_2 NPs with NOM coating (pH 7 to 7.5) gained a negative surface charge attributable to the deprotonated carboxyl groups of the adsorbed NOM. In MHW, cations (particularly Ca^{2+}) can provide charge screening or neutralization, resulting in a less negative charge.[32] After washing into 10 mM phosphate buffer (pH 8), all NPs showed similarly strong negative surface charge ($\zeta < -40$ mV), indicative of phosphate adsorption. It is noted that bare TiO_2 NPs in MHW (pH 8.5) had ζ near zero, resulting in the formation of large NP agglomerates. Thus, we did not proceed with further testing of uncoated NPs in MHW for the degradation studies, as a difference in NP agglomeration state could influence the generation of ROS.[33]

ATR-FTIR was used to assess interactions between the MHW ions, NOM, and TiO_2 NPs (ESI† Fig. S2–S4). A strong phosphate peak at wavenumber ν = 1077 cm^{-1} was observed in all samples that received phosphate treatment. The possibilities for adsorption of HCO_3^- from MHW and precipitation of calcium phosphate species when transferring from MHW to phosphate buffer were also assessed. The FTIR spectra showed no observable formation of calcium phosphate (hydroxyapatite) peaks[34] (ESI† Fig. S2), which was also confirmed by XRD analysis (ESI† Fig. S5). Bicarbonate adsorption from MHW was observed but was then displaced upon phosphate exposure (ESI† Fig. S2). For the NOM, characteristic absorption bands representing the asymmetric and symmetric stretch of the deprotonated COO^- groups were observed in the $\nu \approx 1580$ cm^{-1} and 1400 cm^{-1} regions, respectively, with the peak spacing between these two bands, $\Delta\nu$, indicative of the binding modes.[35–38] To evaluate binding mode, comparison against the "ionic" peak spacing, $\Delta\nu_{ionic}$, is required, where $\Delta\nu_{ionic}$ was measured on NOM alone dry deposited from DIW (ESI† Fig. S3a). The NOM adsorbed to TiO_2 in DIW showed a larger peak spacing than $\Delta\nu_{ionic}$ consistent with bidentate bridging[35] onto the TiO_2 surface. In MHW, a smaller peak spacing was observed which is indicative of bidentate chelating;[36] however, the control NOM sample in MHW without TiO_2 also showed similar peak spacing, suggesting the chelating is likely attributable to NOM–Ca^{2+} interactions in solution and not necessarily the TiO_2 surface interaction. Prior studies have similarly reported that Ca^{2+} can induce both aggregation of the deprotonated NOM and/or bridge the negatively charged NOM to TiO_2.[22,39,40] After phosphate treatment, significant desorption was observed for both NOM layers (ESI† Fig. S4).

To quantify and identify the initial adsorbed species and those displaced by phosphate, the supernatants collected from the batch samples from the initial NOM adsorption and subsequent two washes in phosphate buffer were further analyzed. Solution depletion analysis (*i.e.*, subtracting the remaining from the initial NOM) of batch TOC measurements yielded initial adsorbed masses of 50 mg g^{-1} (0.92 mg m^{-2}) and 11 mg g^{-1} (0.20 mg m^{-2}) in MHW and DIW, respectively. The higher NOM adsorption in MHW is attributed to the calcium ions in MHW, which can induce bridging of NOM to the TiO_2 surface.[21,22] For a more detailed analysis of which species from the NOM mixture adsorbed initially and desorbed in the phosphate washes, SEC measurements were performed. The raw SEC-UV-dRI chromatograms of the unadsorbed or desorbed NOM in the supernatants are shown in ESI† Fig. S6. The initial adsorbed NOM fraction was obtained by taking difference chromatograms of the initial NOM and unadsorbed NOM after depletion onto the TiO_2 NPs (Fig. 1). The initial NOM adsorbed in MHW and DIW was estimated to be 73 ± 4 mg g^{-1} (1.34 ± 0.07 mg m^{-2}) and 23 ± 4 mg g^{-1} (0.42 ± 0.08 mg m^{-2}) respectively, based on UV detection (n = 4 replicate experiments) (details in the ESI† eqn (S1)). The higher adsorbed mass estimate compared to TOC analysis is likely attributable to adsorptive fractionation, where more aromatic (UV-absorbing) species are depleted disproportionately to other species.[23,41] As SEC provides the molecular weight distribution with larger species eluting prior to smaller compounds, Fig. 1 further shows the adsorption of a wide range of NOM molecular weights in MHW, whereas most of the adsorbed NOM in DIW was from the moderate molecular weight fraction. Although SEC-dRI analysis was also conducted (ESI† Fig. S6b), the lower signal and coelution with solvent peaks precluded quantification of the total adsorbed mass.

Desorption into the phosphate washes was evaluated directly in the supernatant of the wash steps (ESI† Fig. S6), and the remaining adsorbed NOM was computed by difference (details in the ESI† eqn (S2) and eqn (S3)). NOM desorption by phosphate buffer reduced the adsorbed NOM concentration to 44 ± 2 mg g^{-1} (*i.e.*, 60 ± 6% of the initial layer remaining) and 8 ± 2 mg g^{-1} (*i.e.*, 38 ± 15% of the initial layer remaining) in MHW and DIW, respectively (n = 3 replicate experiments). Phosphate washes resulted in desorption of primarily the moderate molecular weight fractions from both the NOM_{DIW} and the NOM_{MHW} layers (Fig. 1). Overall, it can be concluded that different adsorbed masses and species of NOM species were adsorbed in DIW and MHW, and that these differences persisted even after partial displacement of the NOM by phosphate.

Influence of remaining NOM coating layers on phenol degradation and byproduct formation

The reactivity of the NOM-coated TiO_2 NPs is hypothesized to potentially be influenced by the total adsorbed mass of NOM, as well as its composition and conformation. The photocatalytic degradation and byproduct formation for 20 mg L^{-1} phenol (Fig. 2) and 50 mg L^{-1} phenol (Fig. 3) were compared using TiO_2–no NOM, TiO_2–NOM_{DIW}, and TiO_2–NOM_{MHW} in 10 mM phosphate buffer. It is noted that in photodegradation experiments without phosphate treatment, the TiO_2 NPs without NOM agglomerate substantially over the course of the 300 min photodegradation experiments (z-average hydrodynamic diameter ≫1 μm by DLS) because of charge neutralization or screening, either directly by Ca^{2+} in the case of the MHW background or because of phenol byproduct formation (likely organic acids)[42–46] that can adsorb and neutralize the positive TiO_2 NP surface charge in DI water (below the isoelectric point of the NPs). Hence, only phosphate-treated NPs are compared where no significant changes in pH or DLS size of the NPs were observed after 300 min of irradiation in the phosphate buffer.

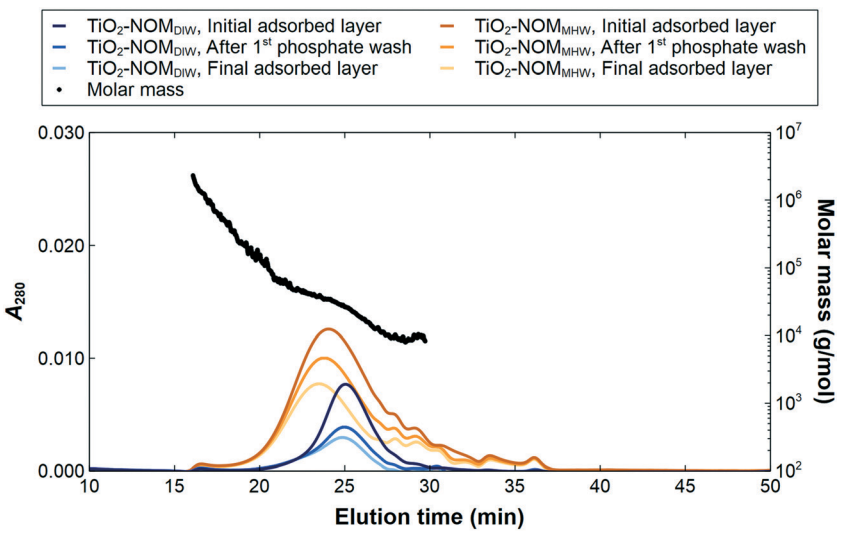

Fig. 1 NOM species adsorbed to the TiO_2 NPs from DIW or MHW, before and after phosphate washes, as identified by difference chromatogram analysis of SEC-UV data. The estimated molar mass of NOM across the elution time was determined by SEC with multi-angle light scattering (MALS) on a 3 g L^{-1} NOM sample (method details in the ESI†).

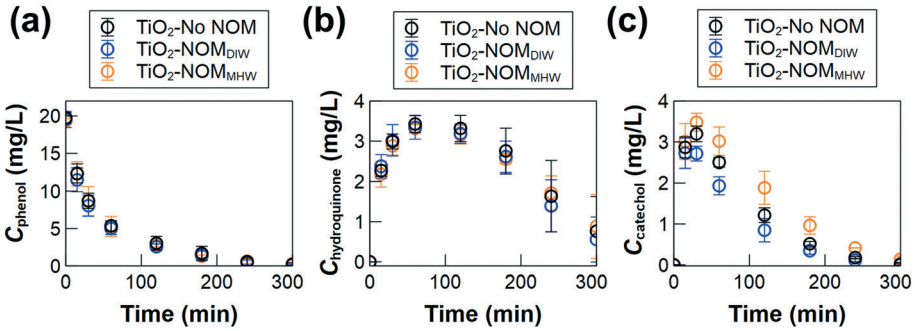

Fig. 2 Degradation of 20 mg L^{-1} phenol (a), and formation and/or degradation of hydroquinone (b) and catechol (c) using 100 mg L^{-1} of TiO_2–no NOM, TiO_2–NOM_{DIW}, or TiO_2–NOM_{MHW} (all in 10 mM phosphate buffer). No phenol losses were observed in dark controls after 300 min (not shown). Error bars represent standard deviation across triplicate experiments.

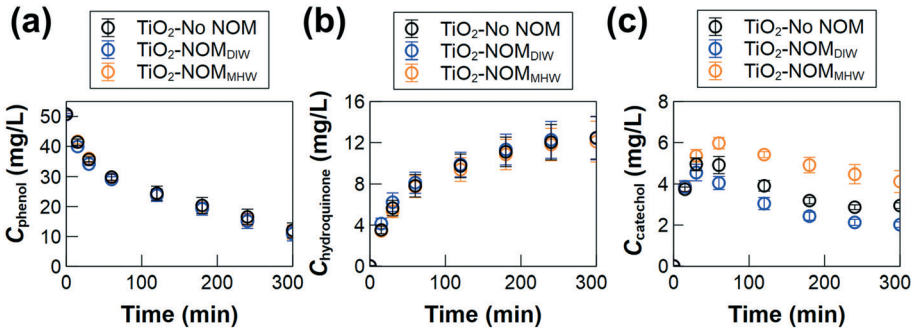

Fig. 3 Degradation of 50 mg L^{-1} phenol (a), and formation and/or degradation of hydroquinone (b) and catechol (c) using 100 mg L^{-1} of TiO_2–no NOM, TiO_2–NOM_{DIW}, or TiO_2–NOM_{MHW} (all in 10 mM phosphate buffer). No phenol losses were observed in dark controls after 300 min (not shown). Error bars represent standard deviation across triplicate experiments.

For phenol itself, no significant differences were observed in the rate of degradation between any of the cases (Fig. 2a and 3a). Further investigations of the response of the two immediate oxidation byproducts of phenol – hydroquinone and catechol – were conducted to more comprehensively evaluate differences in reactivity. Here we focus on these early stage byproducts that were identifiable and quantifiable in the LC analysis (example chromatogram and QTOF mass spectra in ESI† Fig. S7a and b); note that further byproducts can also form as the reaction proceeds[24,42–49] but could not be quantified here if external standards were not commercially available. However, the overall mineralization efficiency was measured by TOC removal after 300 min of irradiation was less than 13% for the different TiO_2 NPs (ESI† Fig. S8). Considering that the contribution of carbon from the remaining adsorbed NOM was 0.31 ± 0.07 mg C per L and 1.74 ± 0.09 mg C per L for TiO_2–NOM_{DIW} and TiO_2–NOM_{MHW}, respectively, compared to the added phenol contribution of 38.3 mg C per L, the TOC is primarily from phenol and its byproducts formed in the mineralization process. A mole balance for the three measured phenolic compounds (ESI† Fig. S9) accounted for <60% of the measured TOC at the end of the 300 min experiments, indicating that a significant amount of other byproducts are also present in the samples. Dark controls for the NPs with phenol and NP-free controls (irradiated mixtures of phenol, catechol, or hydroquinone and 5 mg L^{-1} of NOM) showed no significant losses of phenol and no significant production of the byproducts of interest over the 300 min experiment.

Similar to phenol, there was no difference in the formation or degradation of hydroquinone with the different NOM layers (Fig. 2b and 3b). On the contrary, the degradation profile of catechol was not only distinct in the different NOM-coated TiO_2 NPs, but the two coatings induced *opposite* effects on the reactivity: TiO_2–NOM_{DIW} showed enhanced catechol degradation, whereas TiO_2–NOM_{MHW} showed suppressed catechol degradation (Fig. 2c and 3c). To explore and eliminate the possible role of bicarbonate ions in the TiO_2–NOM_{MHW} samples, studies were also conducted using TiO_2 NPs exposed to $NaHCO_3$ before phosphate treatment. Prior studies have reported contradictory results on the effects of bicarbonate. Bicarbonate can enhance degradation,[50] *e.g. via* increased hole generation particularly at low concentrations,[3] or by scavenging electrons to enhance hole longevity, leading to overall higher hydroxyl radical formation.[51] However, other studies contradictorily reported that bicarbonate can scavenge holes[52] and quench hydroxyl radicals[3,5] to form bicarbonate radicals and thus have an inhibitory effect on the TiO_2 reactivity. In the present study, the degradation of phenol, as well as the formation and/or degradation of hydroquinone and catechol, using TiO_2 exposed to bicarbonate was similar to bare TiO_2, suggesting that bicarbonate ions did not significantly influence

the rate of degradation here (ESI† Fig. S10), which is consistent with the fact that phosphate treatment displaces the bicarbonate (ESI† Fig. S2). Hence, the key differences observed for TiO_2–NOM_{MHW} are attributable to the NOM coating (not the MHW exposure).

Overall, the results for phenol loss are consistent with those reported by Long *et al.*[18] that phosphate can mitigate the inhibitory effect of NOM. However, the distinctive effects of the two NOM layers on catechol degradation suggest that (1) catechol reacts by a different degradation pathway and/or interacts differently with the adsorbed NOM than phenol or hydroquinone, and (2) differences in the NOM layer properties can persist and influence the NP reactivity even after phosphate treatment.

Differences in catechol degradation are mediated by physical blocking and differences in ROS speciation for NOM_{MHW} layers and enhanced hole reactivity for NOM_{DIW} layers

We hypothesized that catechol may be undergoing specific surface reactions (as opposed to reaction with more highly reactive ROS such as hydroxyl radical) and hence be more significantly influenced by differences in the NOM surface coatings. Indeed, prior studies have reported that catechol can degrade through oxidation by holes whereas phenol and hydroquinone degradation are hydroxyl radical mediated.[17,53]

To further evaluate this hypothesis, we first studied the degradation using 20 mg L^{-1} catechol alone (*i.e.*, not as a byproduct of phenol oxidation). Unlike the catechol produced in the phenol degradation experiments, no significant differences were observed for pure catechol between the bare or coated TiO_2 NPs (ESI† Fig. S11). This result could be attributable to the lack of competition with phenol and other byproducts for ROS and/or surface sorption sites, and hence exacerbated differences among the TiO_2 NPs with different NOM coatings in the phenol reaction experiments. Adsorption studies of each contaminant (phenol, hydroquinone, and catechol) to the TiO_2 NPs without light exposure were thus conducted to investigate potential differences in the physical interaction with surface sites with the different NOM coatings. Further experiments to probe for holes and various types of ROS were also performed without phenol to directly evaluate the reaction modes of the TiO_2 NPs themselves, without interference from phenol or its byproducts.

Adsorptive interactions. It has been well-established that the adsorptive interaction is critical for direct oxidation by holes[17] or surface-localized ROS species. Hence, the adsorption of phenol, hydroquinone, and catechol on the different TiO_2 NPs was evaluated (Fig. 4). Comparing the three compounds in general across all the bare and coated NPs, there was no measurable adsorption of phenol, in agreement with prior studies indicating the absence of phenol adsorption to TiO_2 surface because of a lack of stereochemical configuration that favors adsorption.[54] Rather, catechol showed the highest degree of adsorption compared to phenol and hydroquinone (Fig. 4). These results are also in agreement with previous studies showing an effect of the position of the hydroxylation on adsorption to TiO_2: the *ortho* hydroxyl position (catechol) was found to favor adsorption through surface chelate coordination, while the *para* position (hydroquinone) showed lower adsorption.[17,55]

Comparing the different TiO_2 surface chemistries, TiO_2–NOM_{MHW} showed the lowest catechol and hydroquinone adsorption between the different TiO_2 NPs (with a significant difference at >95% confidence compared to TiO_2–no NOM, p = 0.012 and 0.017 for catechol and hydroquinone, respectively), which could be attributed to the higher adsorbed mass of NOM and hence thicker or less patchy NOM layer, resulting in more limited available surface sites for adsorption and reaction of the catechol at the TiO_2 surface, and hence the longer persistence of catechol for TiO_2–NOM_{MHW} in the phenol degradation studies (Fig. 2c and 3c). However, no significant difference in catechol adsorption was observed between TiO_2–no NOM and TiO_2–NOM_{DIW} (p = 0.61) that could explain the enhanced reactivity of TiO_2–NOM_{DIW} toward catechol. Hence, to more fully evaluate the mechanisms influencing differences in catechol degradation between the TiO_2 NPs, further investigations on ROS generation and hole generation were conducted.

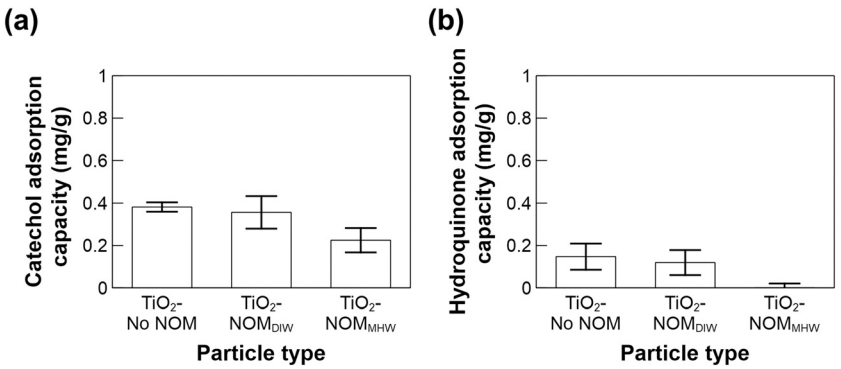

Fig. 4 Adsorbed mass of catechol (a) and hydroquinone (b) onto TiO_2–no NOM, TiO_2–NOM_{DIW}, and TiO_2–NOM_{MHW} from 5 mg L^{-1} initial concentrations of the catechol and hydroquinone in 10 mM phosphate buffer. Error bars represent standard deviation across triplicate experiments.

Generation of reactive oxygen species. Singlet oxygen generation by the TiO_2–no NOM, TiO_2–NOM_{DIW} and TiO_2–NOM_{MHW} was evaluated using furfuryl alcohol as a probe compound; no significant difference was observed across any of the NPs (ESI† Fig. S12). However, distinctive results were obtained by EPR spectroscopy using BMPO to trap transient radical species[56,57] generated during 10 min of UV irradiation (Fig. 5). In the reactions with TiO_2–no NOM and TiO_2–NOM_{DIW}, the trapped radical species were predominately hydroxyl radical (Fig. 5a and b). The BMPO–OH adduct existed in an equilibrium of two conformers, with the same *g* value but slightly different hyperfine splittings (ESI† Fig. S13), giving rise to the overall symmetric EPR lineshape (Fig. 5a and b). On the other hand, in the reaction with TiO_2–NOM_{MHW}, the EPR lineshape of the BMPO-radical adduct(s) was asymmetric indicating that different radical species were trapped (Fig. 5c). Significantly lower radical species were trapped in the reaction with TiO_2–NOM_{MHW} (Fig. 5c). Therefore, in addition to the lower physical adsorption of catechol to the TiO_2–NOM_{MHW}, different types of radical species generated at lower level may contribute to the slower degradation of catechol by TiO_2–NOM_{MHW}. However, similar amounts of radical were trapped in the reactions with TiO_2–no NOM and TiO_2–NOM_{DIW} (Fig. 5a and b), and hence the enhanced reactivity of TiO_2–NOM_{DIW} could not be explained by ROS as probed here.

Hole generation. Holes can induce the oxidation of pollutants by direct electron transfer at the NP surface.[17] The holes were quantified by a starch-iodine assay to quantify iodine produced from the reaction of 5 mM KI. Notably, TiO_2–NOM_{DIW} showed enhanced hole generation compared to TiO_2–No NOM and TiO_2–NOM_{MHW} (Fig. 6). Prior studies reported that positively charged NOM radicals can be produced by electron transfer between electron donating and accepting moieties within NOM or photoionization of NOM that results in loss of electrons[14,15] and hence act as additional holes. Therefore, an enhancement in direct hole oxidation of catechol can explain the increased catechol degradation using TiO_2–NOM_{DIW}. However, no increase or decrease in hole generation was observed in TiO_2–NOM_{MHW} relative to TiO_2–No NOM. Because the TiO_2–NOM_{MHW} coating was comprised of high and low molecular weight species, in addition to the moderate molecular weight species observed in NOM_{DIW}, it is possible that either the specific conformation of the NOM_{MHW} layer is not conducive to enhanced electron transfer, or any enhanced formation of holes or positively-charged radicals is countered by scavenging from the additional NOM species adsorbed in TiO_2–NOM_{MHW}.

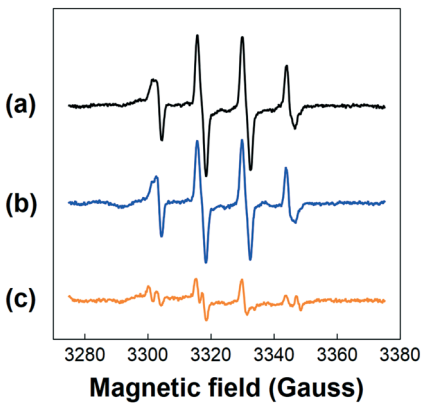

Fig. 5 EPR spectra of BMPO-radical adduct(s) formed in the UV irradiation reactions with TiO_2–no NOM (a); TiO_2–NOM_{DIW} (b); and TiO_2–NOM_{MHW} (c).

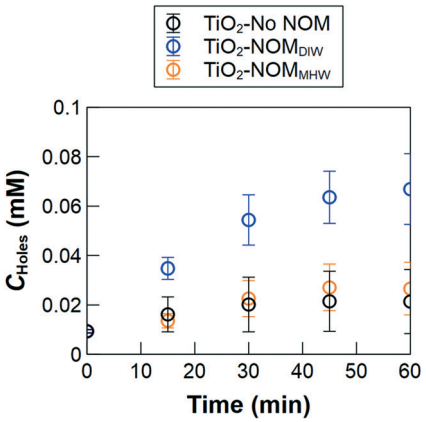

Fig. 6 Quantification of holes generated upon irradiation of the TiO_2 NPs in 10 mM phosphate. Error bars represent standard deviation across four replicate experiments.

Conclusions and implications

This study identified that the detailed properties of adsorbed NOM coatings, including differences in adsorptive fractionation from a single type of NOM (*e.g.*, Suwannee River NOM) in different water chemistry (DIW and MHW), can have persistent influences on the reactivity of TiO_2 NPs even after partial displacement of the NOM by phosphate. Although phenol degradation was not impacted by the residual NOM after phosphate treatment of the bare or NOM-coated particles, the degradation of its catechol byproduct was either enhanced or suppressed, depending on the NOM adsorption condition. These findings imply that evaluation of only a single "model" probe compound such as phenol may preclude a full understanding of the photocatalytic reactivity, whereas byproduct analysis provides additional insights into a wider range of reaction pathways. Furthermore, this study demonstrated that a mechanistic explanation for differences in the photoreactivity of NOM-coated nanoparticles required consideration of not only the ROS species generated, but also direct surface interactions with the NPs, both physical adsorption of catechol, and direct electron transfer interactions such as hole formation. These considerations can be important in the application of photoreactive nanoparticles, as the overall hazard profile of the treated water will require an understanding not only of the removal

of the original pollutants but also the types and persistence of byproducts formed.

Conflicts of interest

There are no conflicts to declare.

Acknowledgements

We gratefully acknowledge Dr. Michael Harold for FTIR instrument access, Dr. Vincent A. Hackley for the NIST SRM 1898 TiO_2 NPs, Dr. Gregory V. Lowry for the SEC column, and Dr. Charisma Lattao for general lab assistance. This material is based upon work supported by the National Science Foundation under Grant No. 1705511. Any opinions, findings, and conclusions or recommendations expressed in this material are those of the authors and do not necessarily reflect the views of the National Science Foundation.

References

1 D. Friedmann, C. Mendive and D. Bahnemann, TiO_2 for water treatment: Parameters affecting the kinetics and mechanisms of photocatalysis, *Appl. Catal., B*, 2010, **99**, 398–406.
2 D. Awfa, M. Ateia, M. Fujii and C. Yoshimura, Novel Magnetic Carbon Nanotube-TiO_2 Composites for Solar Light Photocatalytic Degradation of Pharmaceuticals in the Presence of Natural Organic Matter, *J. Water Process. Eng.*, 2019, **31**, 100836.
3 J. Farner Budarz, A. Turolla, A. F. Piasecki, J.-Y. Bottero, M. Antonelli and M. R. Wiesner, Influence of Aqueous Inorganic Anions on the Reactivity of Nanoparticles in TiO_2 Photocatalysis, *Langmuir*, 2017, **33**, 2770–2779.
4 T. Makropoulou, I. Kortidis, K. Davididou, D. E. Motaung and E. Chatzisymeon, Photocatalytic facile ZnO nanostructures for the elimination of the antibiotic sulfamethoxazole in water, *J. Water Process. Eng.*, 2020, **36**, 101299.
5 R. Yuan, Y. Zhu, B. Zhou and J. Hu, Photocatalytic oxidation of sulfamethoxazole in the presence of TiO_2: Effect of matrix in aqueous solution on decomposition mechanisms, *Chem. Eng. J.*, 2019, **359**, 1527–1536.
6 Y.-M. Kang, M.-K. Kim and K.-D. Zoh, Effect of nitrate, carbonate/bicarbonate, humic acid, and H_2O_2 on the kinetics and degradation mechanism of Bisphenol-A during UV photolysis, *Chemosphere*, 2018, **204**, 148–155.
7 D. Awfa, M. Ateia, M. Fujii and C. Yoshimura, Photocatalytic degradation of organic micropollutants: Inhibition mechanisms by different fractions of natural organic matter, *Water Res.*, 2020, **174**, 115643.
8 L. Gao, B. Zhou, F. Wang, R. Yuan, H. Chen and X. Han, Effect of dissolved organic matters and inorganic ions on TiO_2 photocatalysis of diclofenac: mechanistic study and degradation pathways, *Environ. Sci. Pollut. Res.*, 2020, **27**, 2044–2053.
9 L. Hu, P. M. Flanders, P. L. Miller and T. J. Strathmann, Oxidation of sulfamethoxazole and related antimicrobial agents by TiO_2 photocatalysis, *Water Res.*, 2007, **41**, 2612–2626.
10 J. Brame, M. Long, Q. Li and P. Alvarez, Inhibitory effect of natural organic matter or other background constituents on photocatalytic advanced oxidation processes: Mechanistic model development and validation, *Water Res.*, 2015, **84**, 362–371.
11 H. Wu, L. Huang, A. Rose and V. H. Grassian, Impact of surface adsorbed biologically and environmentally relevant coatings on TiO_2 nanoparticle reactivity, *Environ. Sci.: Nano*, 2020, **7**, 3783–3793.
12 J. M. Farner, R. S. Cheong, E. Mahé, H. Anand and N. Tufenkji, Comparing TiO_2 nanoparticle formulations: stability and photoreactivity are key factors in acute toxicity to Daphnia magna, *Environ. Sci.: Nano*, 2019, **6**, 2532–2543.
13 S. Garg, A. L. Rose and T. D. Waite, Photochemical production of superoxide and hydrogen peroxide from natural organic matter, *Geochim. Cosmochim. Acta*, 2011, **75**, 4310–4320.
14 Y. Li, Y. Pan, L. Lian, S. Yan, W. Song and X. Yang, Photosensitized degradation of acetaminophen in natural organic matter solutions: The role of triplet states and oxygen, *Water Res.*, 2017, **109**, 266–273.
15 Y. Zhang, R. Del Vecchio and N. V. Blough, Investigating the Mechanism of Hydrogen Peroxide Photoproduction by Humic Substances, *Environ. Sci. Technol.*, 2012, **46**, 11836–11843.
16 C. S. Uyguner-Demirel, N. C. Birben and M. Bekbolet, Elucidation of background organic matter matrix effect on photocatalytic treatment of contaminants using TiO_2: A review, *Catal. Today*, 2017, **284**, 202–214.
17 D. Zhao, C. Chen, Y. Wang, H. Ji, W. Ma, L. Zang and J. Zhao, Surface Modification of TiO_2 by Phosphate: Effect on Photocatalytic Activity and Mechanism Implication, *J. Phys. Chem. C*, 2008, **112**, 5993–6001.
18 M. Long, J. Brame, F. Qin, J. Bao, Q. Li and P. J. J. Alvarez, Phosphate Changes Effect of Humic Acids on TiO_2 Photocatalysis: From Inhibition to Mitigation of Electron–Hole Recombination, *Environ. Sci. Technol.*, 2017, **51**, 514–521.
19 M. Erhayem and M. Sohn, Stability studies for titanium dioxide nanoparticles upon adsorption of Suwannee River humic and fulvic acids and natural organic matter, *Sci. Total Environ.*, 2014, **468–469**, 249–257.
20 I. Sit, H. Wu and V. H. Grassian, Environmental Aspects of Oxide Nanoparticles: Probing Oxide Nanoparticle Surface Processes Under Different Environmental Conditions, *Annu. Rev. Anal. Chem.*, 2021, **14**, 9.
21 J. E. Kilduff, T. Karanfil and W. J. Weber, Competitive Interactions among Components of Humic Acids in Granular Activated Carbon Adsorption Systems: Effects of Solution Chemistry, *Environ. Sci. Technol.*, 1996, **30**, 1344–1351.
22 M. Luo, Y. Huang, M. Zhu, Y.-n. Tang, T. Ren, J. Ren, H. Wang and F. Li, Properties of different natural organic

matter influence the adsorption and aggregation behavior of TiO_2 nanoparticles, *J. Saudi Chem. Soc.*, 2018, **22**, 146–154.

23 S. Shakiba, A. Hakimian, L. R. Barco and S. M. Louie, Dynamic Intermolecular Interactions Control Adsorption from Mixtures of Natural Organic Matter and Protein onto Titanium Dioxide Nanoparticles, *Environ. Sci. Technol.*, 2018, **52**, 14158–14168.

24 D. Vione, T. Picatonotto and M. E. Carlotti, Photodegradation of phenol and salicylic acid by coated rutile-based pigments: a new approach for the assessment of sunscreen treatment efficiency, *J. Cosmet. Sci.*, 2003, **54**, 513–524.

25 K. Lv, X. Guo, X. Wu, Q. Li, W. Ho, M. Li, H. Ye and D. Du, Photocatalytic selective oxidation of phenol to produce dihydroxybenzenes in a TiO_2/UV system: Hydroxyl radical versus hole, *Appl. Catal., B*, 2016, **199**, 405–411.

26 National Institute of Standards and Technology (NIST). Certificate of Analysis: SRM 1898 - Titanium dioxide nanomaterials, Gaithersburg, MD, 2020.

27 S. Li and J. Hu, Transformation products formation of ciprofloxacin in UVA/LED and UVA/LED/TiO_2 systems: Impact of natural organic matter characteristics, *Water Res.*, 2018, **132**, 320–330.

28 X. Cheng, H. Guo, Y. Zhang, X. Wu and Y. Liu, Non-photochemical production of singlet oxygen via activation of persulfate by carbon nanotubes, *Water Res.*, 2017, **113**, 80–88.

29 S. M. Louie, R. D. Tilton and G. V. Lowry, Effects of Molecular Weight Distribution and Chemical Properties of Natural Organic Matter on Gold Nanoparticle Aggregation, *Environ. Sci. Technol.*, 2013, **47**, 4245–4254.

30 Z. Li, S. Shakiba, N. Deng, J. Chen, S. M. Louie and Y. Hu, Natural Organic Matter (NOM) Imparts Molecular-Weight-Dependent Steric Stabilization or Electrostatic Destabilization to Ferrihydrite Nanoparticles, *Environ. Sci. Technol.*, 2020, **54**, 6761–6770.

31 S. M. Louie, E. R. Spielman-Sun, M. J. Small, R. D. Tilton and G. V. Lowry, Correlation of the Physicochemical Properties of Natural Organic Matter Samples from Different Sources to Their Effects on Gold Nanoparticle Aggregation in Monovalent Electrolyte, *Environ. Sci. Technol.*, 2015, **49**, 2188–2198.

32 H. Zhang, W. Wang, H. Zhao, L. Zhao, L.-Y. Gan and L.-H. Guo, Facet-mediated interaction between humic acid and TiO_2 nanoparticles: implications for aggregation and stability kinetics in aquatic environments, *Environ. Sci.: Nano*, 2019, **6**, 1754–1764.

33 D. Jassby, J. Farner Budarz and M. Wiesner, Impact of Aggregate Size and Structure on the Photocatalytic Properties of TiO_2 and ZnO Nanoparticles, *Environ. Sci. Technol.*, 2012, **46**, 6934–6941.

34 E. Ahounbar, S. M. Mousavi Khoei and H. Omidvar, Characteristics of in-situ synthesized Hydroxyapatite on TiO_2 ceramic via plasma electrolytic oxidation, *Ceram. Int.*, 2019, **45**, 3118–3125.

35 S. Jayalath, H. Wu, S. C. Larsen and V. H. Grassian, Surface Adsorption of Suwannee River Humic Acid on TiO_2 Nanoparticles: A Study of pH and Particle Size, *Langmuir*, 2018, **34**, 3136–3145.

36 G. B. Deacon and R. J. Phillips, Relationships between the carbon-oxygen stretching frequencies of carboxylato complexes and the type of carboxylate coordination, *Coord. Chem. Rev.*, 1980, **33**, 227–250.

37 H. Wu, N. I. Gonzalez-Pech and V. H. Grassian, Displacement reactions between environmentally and biologically relevant ligands on TiO2 nanoparticles: insights into the aging of nanoparticles in the environment, *Environ. Sci.: Nano*, 2019, **6**, 489–504.

38 C. C. R. Sutton, G. da Silva and G. V. Franks, Modeling the IR Spectra of Aqueous Metal Carboxylate Complexes: Correlation between Bonding Geometry and Stretching Mode Wavenumber Shifts, *Chem. – Eur. J.*, 2015, **21**, 6801–6805.

39 J. Kim, W. Shan, S. H. R. Davies, M. J. Baumann, S. J. Masten and V. V. Tarabara, Interactions of Aqueous NOM with Nanoscale TiO_2: Implications for Ceramic Membrane Filtration-Ozonation Hybrid Process, *Environ. Sci. Technol.*, 2009, **43**, 5488–5494.

40 X. Z. Li, C. M. Fan and Y. P. Sun, Enhancement of photocatalytic oxidation of humic acid in TiO_2 suspensions by increasing cation strength, *Chemosphere*, 2002, **48**, 453–460.

41 G. V. Korshin, C.-W. Li and M. M. Benjamin, Monitoring the properties of natural organic matter through UV spectroscopy: A consistent theory, *Water Res.*, 1997, **31**, 1787–1795.

42 Z. Guo, R. Ma and G. Li, Degradation of phenol by nanomaterial TiO_2 in wastewater, *Chem. Eng. J.*, 2006, **119**, 55–59.

43 K.-i. Okamoto, Y. Yamamoto, H. Tanaka, M. Tanaka and A. Itaya, Heterogeneous Photocatalytic Decomposition of Phenol over TiO_2 Powder, *Bull. Chem. Soc. Jpn.*, 1985, **58**, 2015–2022.

44 J. Chen, L. Eberlein and C. H. Langford, Pathways of phenol and benzene photooxidation using TiO_2 supported on a zeolite, *J. Photochem. Photobiol., A*, 2002, **148**, 183–189.

45 P. Górska, A. Zaleska and J. Hupka, Photodegradation of phenol by UV/TiO_2 and Vis/N,C-TiO_2 processes: Comparative mechanistic and kinetic studies, *Sep. Purif. Technol.*, 2009, **68**, 90–96.

46 T. T. T. Dang, S. T. T. Le, D. Channei, W. Khanitchaidecha and A. Nakaruk, Photodegradation mechanisms of phenol in the photocatalytic process, *Res. Chem. Intermed.*, 2016, **42**, 5961–5974.

47 A. M. Peiró, J. A. Ayllón, J. Peral and X. Doménech, TIO_2-photocatalyzed degradation of phenol and ortho-substituted phenolic compounds, *Appl. Catal., B*, 2001, **30**, 359–373.

48 A. Sobczyński, Ł. Duczmal and W. Zmudziński, Phenol destruction by photocatalysis on TiO_2: an attempt to solve the reaction mechanism, *J. Mol. Catal. A: Chem.*, 2004, **213**, 225–230.

49 I. Ilisz and A. Dombi, Investigation of the photodecomposition of phenol in near-UV-irradiated aqueous TiO_2 suspensions. II. Effect of charge-trapping species on product distribution, *Appl. Catal., A*, 1999, **180**, 35–45.

50 W. W.-P. Lai, M.-H. Hsu and A. Y.-C. Lin, The role of bicarbonate anions in methotrexate degradation via UV/TiO_2: Mechanisms, reactivity and increased toxicity, *Water Res.*, 2017, **112**, 157–166.

51 A. Molinari, L. Samiolo and R. Amadelli, EPR spin trapping evidence of radical intermediates in the photo-reduction of bicarbonate/CO_2 in TiO_2 aqueous suspensions, *Photochem. Photobiol. Sci.*, 2015, **14**, 1039–1046.

52 D. E. Santiago, J. Araña, O. González-Díaz, M. E. Alemán-Dominguez, A. C. Acosta-Dacal, C. Fernandez-Rodríguez, J. Pérez-Peña and J. M. Doña-Rodríguez, Effect of inorganic ions on the photocatalytic treatment of agro-industrial wastewaters containing imazalil, *Appl. Catal., B*, 2014, **156–157**, 284–292.

53 X. Li, J. W. Cubbage, T. A. Tetzlaff and W. S. Jenks, Photocatalytic Degradation of 4-Chlorophenol. 1. The Hydroquinone Pathway, *J. Org. Chem.*, 1999, **64**, 8509–8524.

54 S. Tunesi and M. Anderson, Influence of chemisorption on the photodecomposition of salicylic acid and related compounds using suspended titania ceramic membranes, *J. Phys. Chem.*, 1991, **95**, 3399–3405.

55 D. Vasudevan and A. T. Stone, Adsorption of Catechols, 2-Aminophenols, and 1,2-Phenylenediamines at the Metal (Hydr)Oxide/Water Interface: Effect of Ring Substituents on the Adsorption onto TiO_2, *Environ. Sci. Technol.*, 1996, **30**, 1604–1613.

56 N. Khan, C. M. Wilmot, G. M. Rosen, E. Demidenko, J. Sun, J. Joseph, J. O'Hara, B. Kalyanaraman and H. M. Swartz, Spin traps: in vitro toxicity and stability of radical adducts, *Free Radical Biol. Med.*, 2003, **34**, 1473–1481.

57 H. Zhao, J. Joseph, H. Zhang, H. Karoui and B. Kalyanaraman, Synthesis and biochemical applications of a solid cyclic nitrone spin trap: a relatively superior trap for detecting superoxide anions and glutathiyl radicals, *Free Radical Biol. Med.*, 2001, **31**, 599–606.

